

The cleanest of them all: NLO electroweak corrections to vector-boson scattering into doubly polarised ZZ pairs at the LHC

Ansgar Denner,^a Robert Franken,^a Santiago Lopez Portillo Chavez,^a Daniele Lombardi,^b Giovanni Pelliccioli^c

^a*Institut für Theoretische Physik und Astrophysik, Universität Würzburg,
Emil-Hilb-Weg 22, 97074 Würzburg, Germany*

^b*Dipartimento di Fisica, Università di Torino and INFN, Sezione di Torino,
Via P. Giuria 1, 10125 Torino, Italy*

^c*Università degli Studi di Milano–Bicocca and INFN Sezione di Milano–Bicocca,
Piazza della Scienza 3, 20126 Milano, Italy*

E-mail: ansgar.denner@uni-wuerzburg.de, robert.franken@uni-wuerzburg.de,
santiago.lopez-portillo-chavez@uni-wuerzburg.de, daniele.lombardi@unito.it,
giovanni.pelliccioli@unimib.it

ABSTRACT: We present the first calculation of the next-to-leading-order electroweak corrections to vector-boson scattering into doubly polarised Z bosons at the LHC in the fully leptonic decay channel. The production and decay of the two polarised Z bosons are consistently modelled in the double-pole approximation, separating polarisation states at the amplitude level and including factorisable real and virtual electroweak corrections. Doubly polarised and unpolarised signals are investigated and confronted with off-shell results. A broad analysis, including results at integrated and differential level, is carried out in a realistic, CMS-inspired fiducial setup. Our study paves the way to upcoming analyses with LHC Run-3 and High-Luminosity data as well as to further phenomenological investigations.

KEYWORDS: LHC, polarisation, vector-boson scattering, NLO, electroweak

Contents

1	Introduction	1
2	Details of the calculation	2
2.1	Tools and Validation	3
2.2	Input parameters	3
2.3	Event selection	4
3	LHC phenomenology	5
3.1	Integrated results	5
3.2	Differential distributions	6
4	Conclusion	9

1 Introduction

Vector-boson scattering (VBS) plays a key role in probing the electroweak (EW) and scalar sectors of the Standard Model (SM) and, in particular, the mechanism of electroweak-symmetry breaking. Its sensitivity to quartic gauge couplings, which is enhanced by strong gauge cancellations, renders it a powerful laboratory to test the consistency of the SM in the high-energy regime as well as an important probe of beyond-the-SM effects.

Among the various VBS channels accessible at the Large Hadron Collider (LHC), the production of two Z bosons in association with two jets occupies a special position. When the Z bosons decay to charged leptons, the four-lepton final state leads to a remarkably clean experimental signature. At variance with WZ and WW production mechanisms, which involve one or two neutrinos in the final state, in ZZ production all final-state particles can be reconstructed, enabling a precise determination of the event kinematics. Thus, ZZ scattering with four final-state charged leptons is the golden channel for detailed studies of VBS dynamics and especially the analysis of polarisation-sensitive observables. At the same time, the four-lepton channel suffers from a rather small cross section, owing to the small branching ratio of two Z bosons into charged leptons. As a consequence, the experimental measurement is statistically dominated, but an improvement is expected with the upcoming High-Luminosity LHC run, hopefully allowing for polarisation analyses. From the theoretical viewpoint, precise and accurate predictions for ZZ scattering require the inclusion of higher-order perturbative corrections in the EW and the strong (QCD) coupling, a proper treatment of off-shell and interference effects, and the application of realistic fiducial selections to enable a meaningful comparison between real LHC data and numerical SM predictions.

Experimentally, the ZZ scattering into four charged leptons has been investigated [1, 2] and observed [3, 4] with LHC Run-2 data. The low statistics makes the analysis of the polarisation structure of this channel intricate, but prospect studies for the upcoming High-Luminosity upgrade are promising [5].

On the theory side, the next-to-leading-order (NLO) QCD corrections in the SM to both the signal and irreducible background have been known for a long time [6, 7] and also matched to a parton shower [8]. The modelling of the gluon-initiated loop-induced irreducible background has been studied as well [9]. The EW corrections as well as the full tower of NLO corrections to off-shell

ZZ scattering at the LHC have been calculated for both the signal and the irreducible-background processes [10, 11]. All known predictions pertain the final-state signature with four leptons and two jets, i.e. the fully leptonic decay channel, which is also considered in this work. The SM predictions for polarised Z bosons in ZZ scattering are currently limited to leading order (LO) combined with parton-shower simulations via matching and merging techniques in the PHANTOM [12], MADGRAPH5_AMC@NLO [13], and SHERPA [14] Monte Carlo frameworks.

In this work, we analyse the polarisation structure of ZZ scattering in the decay channel with two different-flavour charged-lepton pairs, achieving for the first time NLO accuracy in the EW coupling to both production and decay of polarised Z bosons.

This paper is organised as follows. In Section 2 we describe the considered process, show the results of the validation of our calculation, and detail input parameters and event selections. The integrated and differential results are presented in Section 3 for a realistic fiducial setup. We draw our conclusions in Section 4.

2 Details of the calculation

We consider the LHC signature

$$pp \rightarrow e^+e^-\mu^+\mu^-jj, \quad (2.1)$$

which includes VBS into Z bosons decaying leptonically. The off-shell modelling of this process has been studied in Refs. [10, 11], where a detailed presentation of the contributing partonic channels and of sample Feynman diagrams was given. We restrict ourselves here to the LO and NLO EW terms, i.e. the $\mathcal{O}(\alpha^6)$ and $\mathcal{O}(\alpha^7)$ perturbative orders. The dominant contributions to the cross section originate from quark–quark-induced channels involving quarks of the first two generations. We do not take into account bottom-quark channels, whose impact is at the level of a few percent [10]. Similarly, photon–photon-induced channels are disregarded. At LO, these $\gamma\gamma$ -induced channels contribute at the level of parts-per-million. We do, however, include single-photon-induced channels (γq), which involve contributions with vector-boson-scattering topologies at $\mathcal{O}(\alpha^7)$.

While we compute the full off-shell process in Eq. (2.1), the main target of this work are the *on-shell* signals with either polarised or unpolarised intermediate Z bosons, i.e.

$$pp \rightarrow Z_{\lambda_1}(\rightarrow e^+e^-)Z_{\lambda_2}(\rightarrow \mu^+\mu^-)jj, \quad \lambda_1, \lambda_2 = \text{L, T, U}, \quad (2.2)$$

where the indices L, T, and U label longitudinal, transverse, and unpolarised Z bosons. We stress that the transverse polarisation includes the left–right interference terms, as usually done in experimental analyses that rely on polarised-template fits.

The calculation of the full off-shell process uses the complex-mass scheme [15–18] to treat the vector-boson resonances in a gauge-invariant way. On the other hand, gauge invariance for the on-shell signal processes in Eq. (2.2) is guaranteed by making use of the pole approximation [18–21]. Within this approximation, the polarised signals are defined as specified in Refs. [22–24], where all relevant analytical results can be found. The polarisation states of the massive vector bosons are frame dependent. We choose to define them in the di-boson centre-of-mass frame, which is best motivated from a theoretical point of view [24] and used in recent experimental analyses [25, 26]. Non-factorisable EW corrections, which are expected to be suppressed in the phase-space region dominated by the Z-boson resonances, are neglected.

The subtraction of the infrared (IR) divergences is based on the Catani–Seymour dipole formalism [27–32]. IR singularities originating from the splitting of virtual photons into quark–antiquark pairs are regularised using the photon-to-jet conversion function [33].

The calculation within the double-pole approximation (DPA) requires a tailored dipole selection, which we carry out using the general strategy outlined in Refs. [24, 34] restricted to the case of neutral resonances.

The final state of Eq. (2.2) receives contributions involving three vector-boson resonances, which become sizeable if the invariant mass of the jet pair is close to a vector-boson mass. These contributions are singular in the DPA, where all resonance widths are set to zero in the residue of the amplitude. While at LO such contributions are removed by the cut on the jet-pair invariant mass, Eq. (2.15), this cut can be evaded if a real-emission photon is recombined with one of the jets in radiative events. For the regularisation of these kind of singularities, we use the *fudge-factor scheme* introduced in Ref. [35] and available in MOCANLO [34, 36] and BBMC. To this end, for each potential resonance that is not treated within the pole approximation, the squared matrix element is multiplied by a fudge factor, defined as

$$\mathcal{F}(s_V) = \begin{cases} 1 & |\sqrt{s_V} - M_V| > c_{\mathcal{F}} \Gamma_V \\ \frac{(s_V - M_V^2)^2}{(s_V - M_V^2)^2 + \Gamma_V^2 M_V^2} & |\sqrt{s_V} - M_V| < c_{\mathcal{F}} \Gamma_V \end{cases}, \quad (2.3)$$

where s_V refers to the Lorentz invariant associated with the unprotected resonance V ($= W, Z$) decaying to a quark–antiquark pair, and $c_{\mathcal{F}}$ is some parameter, for which we have chosen $c_{\mathcal{F}} = 3$. Since the fudge factors multiply complete gauge-invariant squared matrix elements, gauge invariance is not violated.

2.1 Tools and Validation

The calculation has been performed with the Monte Carlo integration codes MOCANLO [34, 36] and BBMC. While both use RECOLA [37, 38] and COLLIER [39] for the evaluation of LO and NLO matrix elements, they rely on independent implementations of the phase-space integration based on multi-channel importance sampling according to Refs. [15, 40, 41].

As a validation of our calculation, all numerical results for cross sections and distributions reported in Section 3 have been produced with both integration codes, showing agreement at the few permille level. The results for the different contributions of the employed subtraction formalism, i.e. integrated dipole, real and virtual contributions, have been compared and separately agree within the statistical uncertainty of the calculation.

The results presented in Section 3 are based on MOCANLO.

2.2 Input parameters

We have generated results for the Run-3 energy of the LHC, i.e. $\sqrt{s} = 13.6$ TeV. The on-shell values for masses and widths of EW bosons are taken from the PDG review [42],

$$\begin{aligned} M_Z^{\text{OS}} &= 91.1880 \text{ GeV}, & \Gamma_Z^{\text{OS}} &= 2.4955 \text{ GeV}, \\ M_W^{\text{OS}} &= 80.3692 \text{ GeV}, & \Gamma_W^{\text{OS}} &= 2.085 \text{ GeV}, \end{aligned} \quad (2.4)$$

and are converted into pole values ($M_Z, M_W, \Gamma_W, \Gamma_Z$) following Ref. [43], leading to

$$M_Z = 91.153872568 \text{ GeV}, \quad \Gamma_Z = 2.494566050 \text{ GeV}, \quad (2.5)$$

$$M_W = 80.342168302 \text{ GeV}, \quad \Gamma_W = 2.084298723 \text{ GeV}. \quad (2.6)$$

The parameters for the top quark and the Higgs boson read [42]

$$\begin{aligned} m_t &= 172.57 \text{ GeV}, & \Gamma_t &= 1.42 \text{ GeV}, \\ M_H &= 125.20 \text{ GeV}, & \Gamma_H &= 0.0041 \text{ GeV}, \end{aligned} \quad (2.7)$$

where the Higgs width is taken from Ref. [44]. Leptons and light quarks, including the bottom quark, are treated as massless.

The EW coupling is fixed via the G_μ input scheme [21, 45]. For the off-shell calculation this amounts to using

$$\alpha = \frac{\sqrt{2}}{\pi} G_\mu \left| \mu_W^2 \left(1 - \frac{\mu_W^2}{\mu_Z^2} \right) \right|, \quad \mu_V^2 = M_V^2 - iM_V\Gamma_V, \quad V = W, Z, \quad (2.8)$$

with the complex masses μ_V in the complex-mass scheme [16, 17]. Instead, the (un)polarised results in DPA are obtained with the coupling computed from real masses

$$\alpha = \frac{\sqrt{2}}{\pi} G_\mu M_W^2 \left(1 - \frac{M_W^2}{M_Z^2} \right). \quad (2.9)$$

In both cases, the Fermi constant is set to

$$G_\mu = 1.1663788 \times 10^{-5} \text{ GeV}^{-2}. \quad (2.10)$$

Thus, we use the values resulting from Eq. (2.8) and Eq. (2.9),

$$\alpha = 1/132.159951034, \quad \alpha = 1/132.223957653, \quad (2.11)$$

for the off-shell and DPA calculations respectively.

We employ the NNPDF40_nnlo_as_01180_qed [46] PDF set and dynamical renormalisation and factorisation scales,

$$\mu_R = \mu_F = \sqrt{p_{T,j_1} p_{T,j_2}}, \quad (2.12)$$

where p_{T,j_1} and p_{T,j_2} are the transverse momenta of the two jets with highest transverse momenta.

2.3 Event selection

The event selection is adapted from the CMS note [5], in combination with the lepton selection cuts from Ref. [47]. All partons with pseudorapidity $|\eta| > 5$ are assumed to be lost in the beam pipe. For the remaining partons, we apply a two-step recombination procedure. First, we dress leptons with photons with a resolution parameter $R = 0.1$ in the Cambridge–Aachen algorithm [48]. Then, quarks, gluons, and the remaining photons are clustered into jets with a resolution parameter $R = 0.4$ using the anti- k_T algorithm [49].

We require both Z bosons to decay into lepton pairs of different generations, which results in exactly one electron, one positron, one muon, and one antimuon. The four leptons are ordered according to their transverse momenta and labelled ℓ_1 to ℓ_4 . Their respective transverse momenta have to exceed

$$p_{T,\ell_1} > 20 \text{ GeV}, \quad p_{T,\ell_2} > 10 \text{ GeV}, \quad p_{T,\ell_3} > 5 \text{ GeV}, \quad p_{T,\ell_4} > 5 \text{ GeV}. \quad (2.13)$$

The pseudorapidities of all four leptons have to fulfil

$$|\eta_\ell| < 2.5. \quad (2.14)$$

Each same-family lepton–antilepton pair must be inside an invariant mass range of

$$60 \text{ GeV} < M_{\ell^+\ell^-} < 120 \text{ GeV}, \quad (2.15)$$

and the invariant mass of the four-lepton system is bounded by

$$M_{4\ell} > 180 \text{ GeV}. \quad (2.16)$$

Only jets with transverse momentum and pseudorapidity

$$p_{T,j} > 30 \text{ GeV}, \quad |\eta_j| < 4.7 \quad (2.17)$$

mode	$\sigma_{\text{LO}}^{\alpha^6}$ [ab]	$\Delta\sigma_{\text{NLO},q}^{\alpha^7}$ [ab]	$\delta_{\text{NLO},q}$ [%]	$\Delta\sigma_{\text{NLO},\gamma}^{\alpha^7}$ [ab]	$\delta_{\text{NLO},\gamma}$ [%]	$\sigma_{\text{NLO}}^{\alpha^6+\alpha^7}$ [ab]
full	119.83(1)	-21.4(1)	-17.9	1.850(5)	1.5	100.3(1)
unp.	117.32(2)	-20.52(1)	-17.5	1.7985(2)	1.5	98.59(2)
LL	8.9677(2)	-1.288(3)	-14.4	0.12329(3)	1.4	7.802(4)
LT	16.6406(2)	-2.715(4)	-16.3	0.24794(4)	1.5	14.173(9)
TT	72.8492(4)	-13.48(1)	-18.5	1.1488(1)	1.6	60.51(1)
int.	2.22(2)	-0.32(2)	-	0.0305(2)	-	1.93(3)

Table 1: Fiducial integrated cross sections (in ab units) at LO [$\mathcal{O}(\alpha^6)$] (2nd column) and NLO EW corrections [$\mathcal{O}(\alpha^7)$] for ZZ scattering at the LHC. The NLO EW corrections are listed in absolute terms and relative to the LO in the third and fourth columns for the quark-induced contributions only, and in the fifth and sixth columns for the single-photon-induced contributions. Owing to symmetric cuts on the leptons, the TL contribution is identical to the LT one and thus not shown. The seventh column reports the sum of the two computed orders.

are considered. The two hardest jets, also called tagging jets, need to fulfil

$$|\Delta\eta_{j_1 j_2}| > 2.4, \quad M_{j_1 j_2} > 400 \text{ GeV}. \quad (2.18)$$

Furthermore, we require a separation between the tagging jets and each lepton of

$$\Delta R_{j_1 \ell_k}, \Delta R_{j_2 \ell_k} > 0.4, \quad \forall k \in \{1, \dots, 4\}, \quad (2.19)$$

where $\Delta R_{ij} = \sqrt{(\Delta\phi_{ij})^2 + (\Delta\eta_{ij})^2}$ (with $\Delta\phi$ as the azimuthal-angle difference).

3 LHC phenomenology

3.1 Integrated results

In this section we present the integrated cross sections for the polarised and unpolarised ZZ-scattering process defined in Eqs. (2.1)–(2.2) in the fiducial setup described in Section 2.3. In Table 1 we show fiducial cross sections at LO [$\mathcal{O}(\alpha^6)$] and NLO EW order [$\mathcal{O}(\alpha^7)$], highlighting the relative impact of quark-induced and photon-induced contributions to the various polarisation states, as well as to the unpolarised process. The relative NLO EW corrections are defined via

$$\delta_{\text{NLO},i} = \frac{\Delta\sigma_{\text{NLO},i}^{\alpha^7}}{\sigma_{\text{LO}}^{\alpha^6}}. \quad (3.1)$$

While the single-photon-induced contributions are at the 1.5% level and rather independent of the vector-boson polarisation, the corrections to quark-induced partonic processes are driven by the leading EW Sudakov logarithms in the one-loop virtual corrections. The EW Casimir factors multiplying the leading and sub-leading logarithms depend on the polarisation mode of the EW bosons [50], therefore leading to different EW corrections with a similar hierarchy as in other VBS production mechanisms [24, 35]. In particular, the more longitudinal vector bosons are involved, the smaller the negative EW corrections are.

As for the polarisation fractions, defined as

$$f_{k,\lambda\lambda'} = \frac{\sigma_{k,\lambda\lambda'}}{\sigma_{k,\text{unp.}}}, \quad \lambda, \lambda' = \text{L, T}, \quad k = \text{LO, NLO}, \quad (3.2)$$

results similar to those in W^+W^+ [24] and W^+Z scattering [35] are found, with NLO EW corrections only mildly modifying the corresponding LO predictions. The numerical results are shown in

mode	$f_{\text{LO}} [\%]$	$f_{\text{NLO}} [\%]$
full	102.1	101.7
unp.	100.0	100.0
LL	7.6	7.9
LT	14.2	14.4
TT	62.1	61.4
int.	1.9	1.9

Table 2: Fiducial polarisation fractions at LO and NLO EW accuracy, defined as ratios of (un)polarised integrated cross sections over the unpolarised DPA one (unp.).

Table 2. The purely longitudinal component amounts to about 8% of the unpolarised cross section, the mixed ones (summed) to 28%, while the transverse one gives the dominant contribution with more than 60%. This hierarchy is in line with the expected high-energy behaviour in the SM. There, the longitudinal-boson scattering is subject to strong unitarity cancellations between energy-growing pure-gauge and Higgs-mediated contributions. The transverse modes benefit from a larger number of unsuppressed helicity configurations. On the basis of previous results [24], there are good reasons to believe that QCD corrections do not change dramatically the picture of polarisation fractions. Of course, this could only be verified by computing these corrections, which goes beyond the scope of this work.

By subtracting the sum of polarised cross sections from the DPA unpolarised one, we obtain an interference contribution,

$$\sigma_{k,\text{int.}} = \sigma_{k,\text{unp.}} - \sum_{\lambda,\lambda'=\text{L,T}} \sigma_{k,\lambda\lambda'}, \quad k = \text{LO, NLO}, \quad (3.3)$$

which roughly amounts to a positive 2% both at LO and NLO EW. Finally, the difference between the off-shell calculation and the DPA unpolarised one gives genuine off-shell effects (beyond the pole approximation) at the 2% level both at LO and NLO EW.

3.2 Differential distributions

Before showing differential results, we remark that the analysis of ZZ scattering at the LHC in the decay channel with four charged leptons is clearly statistically dominated. In the considered fiducial setup [5], about 300 (unpolarised) signal events are expected with the full High-Luminosity dataset (3000 fb^{-1}), translating into about 20 LL events. This makes the extraction of the LL fraction challenging already at the level of the fiducial measurement. In spite of the signal purity, differential measurements will only be possible by combining different decay channels. Nonetheless, the differential description of ZZ scattering in the four-charged-lepton channel is useful to further understand the process under the lenses of polarisations and spin correlations. Moreover, the purity of this decay channel makes it possible to directly access a plethora of kinematic observables.

In the considered setup, the kinematic selections applied to the charged leptons are symmetric, therefore the two mixed polarisation states give equivalent contributions. More precisely, the TL contribution to an observable depending on some electron and muon properties is equal to the LT contribution to the observable with electron and muon properties interchanged. Therefore, in all figures we only show distributions for the LT state.

We start by presenting transverse-momentum distributions of the leading charged lepton and of the system of four charged leptons in Figure 1. The two observables share many similar features. In the moderate- and large- p_T regime of both observables, all doubly polarised states decrease at the same rate, with a clear hierarchy in the absolute size lead by the TT state, which is approximately

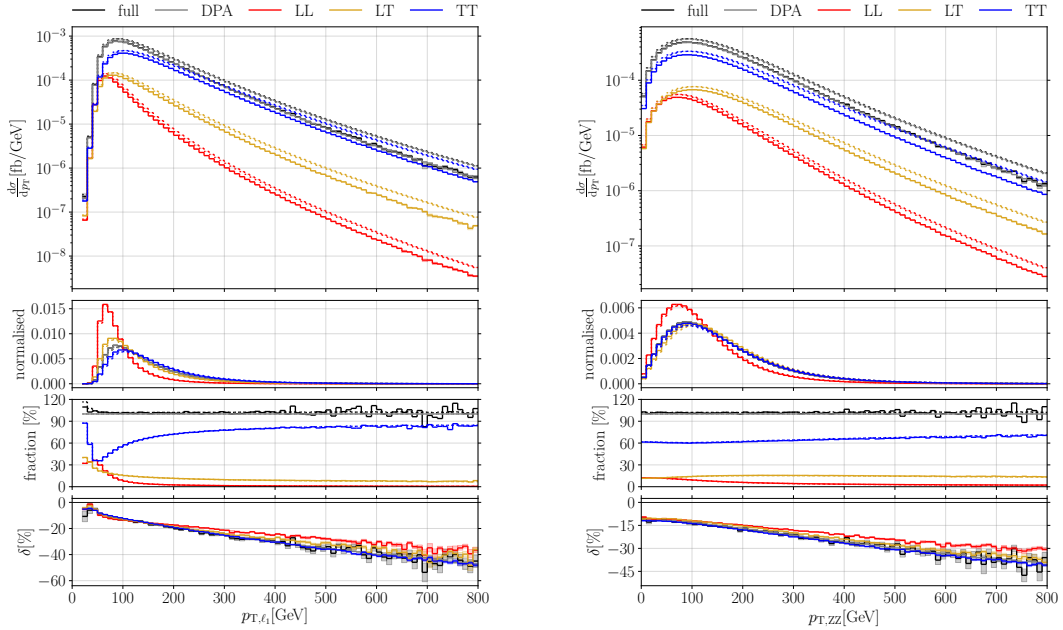


Figure 1: Differential cross section with respect to the transverse momentum of the hardest lepton (left) and the (vectorial) sum of transverse momenta of the four leptons (right). The figure is organised as follows. The top panel shows absolute cross sections, while the second one normalises the cross sections such that the area under all curves equals one. The third panel displays the fraction of the polarisation contribution with respect to the unpolarised DPA cross section. The bottom panel depicts the relative NLO EW corrections in percentages (δ). Solid lines denote the NLO cross section, dashed lines the LO one. Shaded bands indicate the numerical-integration error.

one order of magnitude larger than the mixed states and two orders of magnitude larger than the LL state. In the tails, all LO distributions get increasing negative EW corrections, dominated by large EW Sudakov logarithms appearing in the one-loop SM amplitudes. These negative corrections, which reach up to -40% at $p_{T,ZZ} = 800$ GeV, are slightly larger for the transverse modes of the two Z bosons, owing to a larger EW Casimir factor multiplying the leading Sudakov logarithms compared to the purely longitudinal state. In this region, however, the cross section is roughly three orders of magnitude smaller than in the most populated region. Both transverse-momentum distributions show a marked difference between the purely longitudinal state and all other states in the normalised shapes. Indeed, leptons from longitudinally polarised bosons are preferably emitted orthogonal to the direction of the boson, whereas for transversely polarised bosons the decay products tend to be aligned or anti-aligned with it. Owing to this fact, the LL state populates more the soft part of the p_T spectra, while being more suppressed in the moderate- p_T region. This effect, already found in other VBS production mechanisms [24, 35], makes these transverse-momentum observables suitable for polarisation discrimination, even with a reduced number of bins.

We continue with angular observables associated with the decay leptons, which are expected to inherit in a more direct manner the spin structure of the underlying resonances (the Z bosons) compared to energy-dependent quantities. In Figure 2 we consider the distribution in the cosine of the polar decay angle of the positron in the corresponding Z-boson rest frame, which is the quantity that is most sensitive to the polarisation state of the individual Z boson (the one decaying to the

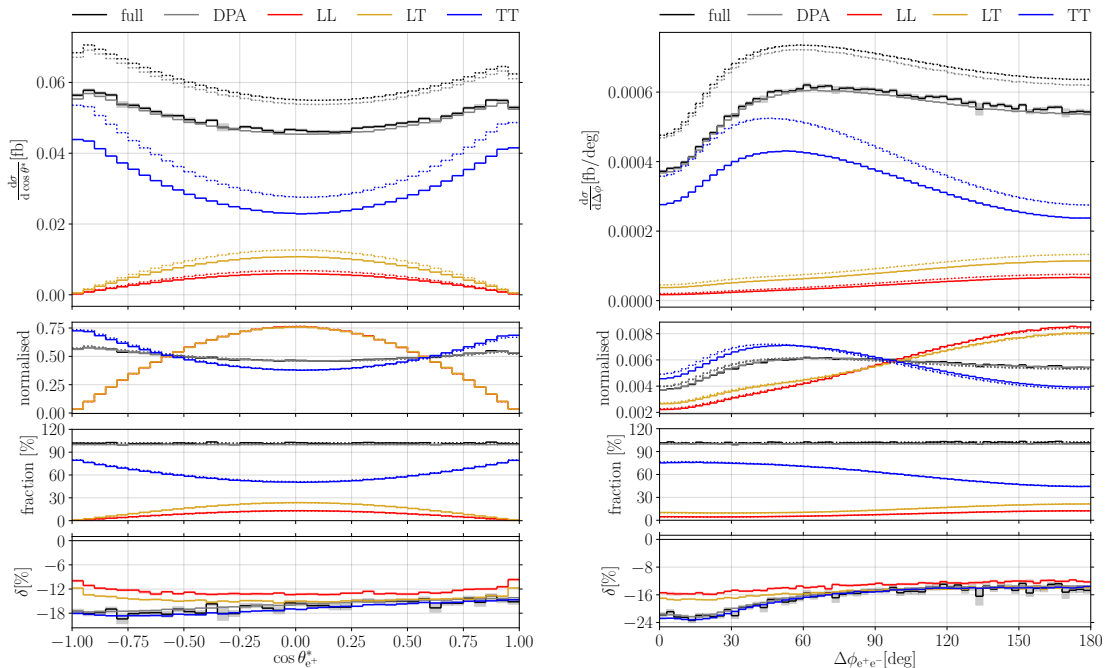


Figure 2: Differential cross section with respect to the cosine of the positron decay angle in the corresponding Z-boson rest frame (left) and to the azimuthal-angle distance between the electron and the positron (right). Same structure as Figure 1.

positron–electron pair) out of the considered observables. At variance with the analogous angle in WZ scattering (see Fig. 5(a) in Ref. [35]), the reconstruction of the positron decay angle only relies on the kinematics of visible particles. Therefore, up to small distortions at the endpoints owing to the loose cuts, the (normalised) distributions show the expected quadratic behaviour with opposite-sign second derivative (negative for LL and LT, positive for TL and TT) [51, 52]. The EW corrections are almost flat and reflect the results at the integrated level.

The distribution in the azimuthal-angle distance (computed in the laboratory frame) between the positron and the electron, presented in the right panels of Figure 2, is strongly correlated with the positron decay angle and therefore possesses a marked discrimination power for the polarisation of the single Z boson. The EW corrections to this quantity are rather flat for $\Delta\phi_{e^+e^-} > 90^\circ$. Below this value they reach up to -25% for the transverse modes (TT, but also TL which is not shown) for $\Delta\phi_{e^+e^-} \rightarrow 0$, while they remain at the -15% level for the longitudinal modes. This behaviour results from the correlation of high-energy Z bosons with small $\Delta\phi_{e^+e^-}$. In fact, smaller $\Delta\phi_{e^+e^-}$ values result from stronger boosted Z bosons, whose higher energy leads to larger EW Sudakov corrections.

In Figure 3 we consider two observables defined as the azimuthal-angle distance between two objects. The one on the left is associated with the two Z bosons (identified as the two same-flavour lepton pairs). While two longitudinal bosons are preferably produced in the same hemisphere, two transverse bosons are dominantly produced in opposite hemispheres, leading to a marked normalised-shape difference between the two states. The mixed polarisation states show a rather flat shape, symmetric about $\Delta\phi_{ZZ} = 90^\circ$. The picture for the azimuthal-angle separation between the two tagging jets is different as shown on the right plot of Figure 3. In this case, the two jets are preferably produced in opposite hemispheres, as usual in processes dominated by vector-boson-

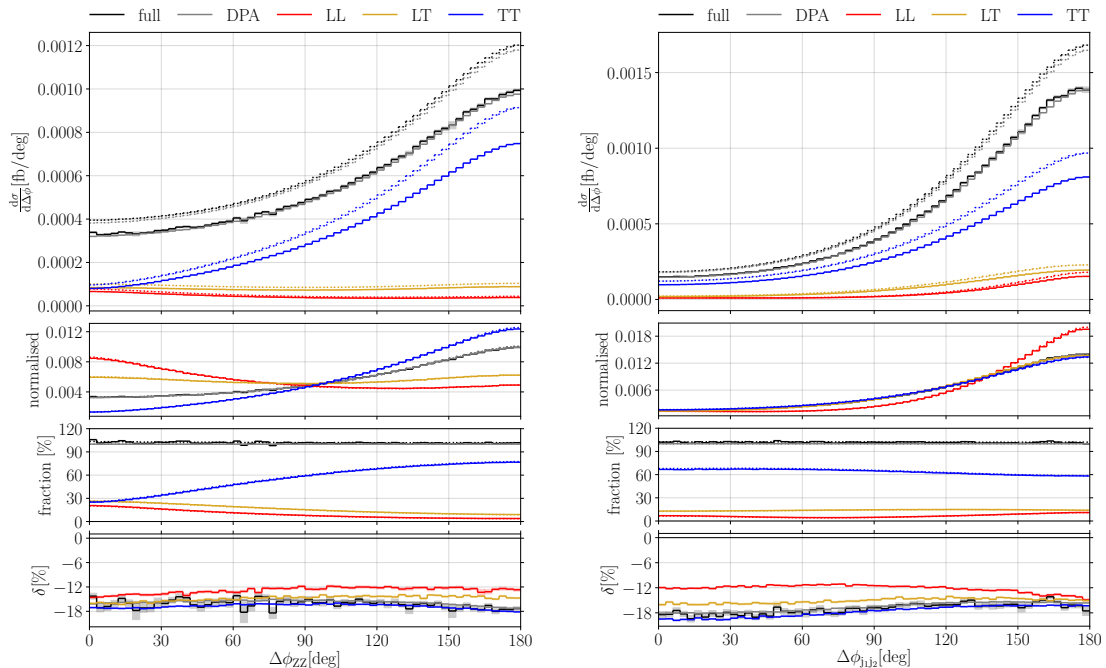


Figure 3: Differential cross section with respect to the azimuthal-angle distance between the two reconstructed Z bosons (left) and between the two tagging jets (right). Same structure as Figure 1.

fusion (VBF) topologies. While this holds for all polarisation states, there is a remaining shape difference between the LL state and all others. This is a clear example of the marked correlation between the spin structure of the di-boson system and the di-jet-system kinematics in VBF topologies. The EW corrections are rather flat for both azimuthal-angle separations. Nevertheless, the differences in EW corrections between the different polarisation modes increase for large $\Delta\phi_{ZZ}$ and small $\Delta\phi_{j_1j_2}$.

In the left panels of Figure 4 we show distributions in the rapidity difference between the two positively charged leptons. This quantity, already studied in the case of same-sign WW production [24], has a fair discrimination power between doubly polarised signals. The TT shape has a maximum at zero rapidity separation, while the LL one is maximal slightly above $\Delta\eta_{e^+\mu^+} = 1$. The EW corrections do not sizeably change the LO distribution shapes.

As a last differential observable, we present in the right panels of Figure 4 the ratio between the transverse momenta of the sub-leading and leading Z bosons $R_{Z_2Z_1} = p_{T,Z_2}/p_{T,Z_1}$. As also seen in WZ scattering [35], the softer transverse-momentum spectrum associated with longitudinal bosons compared to transverse ones leads to a ratio $R_{Z_2Z_1}$ that is typically smaller for the LT compared to the TT state. The EW corrections to this quantity are rather flat for all polarisation states. Nevertheless, for modes involving transverse bosons a slope in the relative corrections is visible.

4 Conclusion

We have achieved for the first time NLO EW accuracy in the electroweak production of two polarised Z bosons in association with two jets at the LHC with subsequent decays to charged leptons.

Specific helicity states of intermediate Z bosons are defined at the level of SM tree-level and one-loop resonant amplitudes, working in the double-pole approximation to ensure both gauge invariance

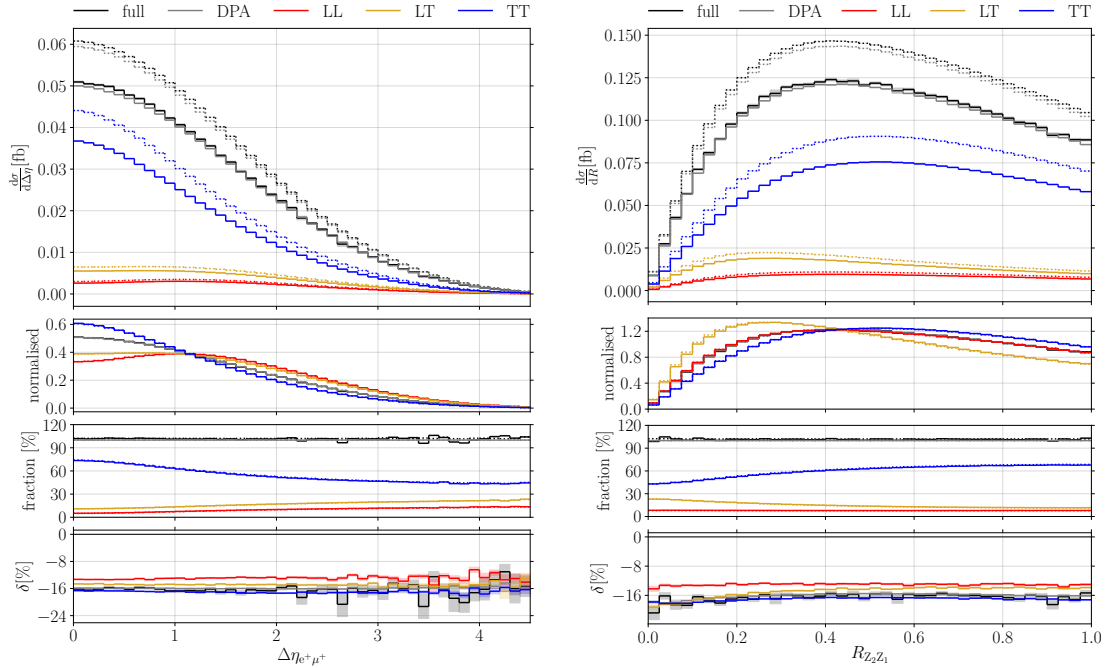


Figure 4: Differential cross section with respect to the rapidity difference between the positron and the antimuon (left) and to the transverse momentum ratio between the subleading and the leading reconstructed Z boson (right). Same structure as Figure 1.

and a sound definition of polarised intermediate states. The factorisable EW corrections to the production and to the decay mechanisms from both real and virtual contributions are consistently combined. This approach makes it possible to estimate both interference and genuine non-resonant effects by comparison with the unpolarised pole-approximated and the full off-shell calculations, respectively.

Large and polarisation-dependent EW corrections are found, ranging from -14% (LL) to -18% (TT) in a realistic CMS-inspired fiducial volume. A number of transverse-momentum and angular observables show a marked discrimination power between doubly polarised ZZ signals and only mild distortions of distribution shapes owing to EW corrections.

This work represents an important advancement for the interpretation of LHC Run-3 data in the clean but statistically limited VBS signature with four charged leptons. We remark that the numerical results shown in this paper can be reproduced with the upcoming public release of version 1.0.1 of the MOCANLO software,

<https://mocanlo.gitlab.io/releases/mocanlo-1.0.1.tar.gz>

using the input cards in the process subfolder

`mocanlo/validated_processes/vbs/zz/pp-zz-ew-ew_pol/`

Acknowledgements

The authors thank Sandro Uccirati and Jean-Nicolas Lang for the maintenance of RECOLA and Claude Charlot, Roberto Covarelli, Lucia Di Ciaccio, Pietro Govoni, Joany Manjarres, Emmanuel Sauvan, Jean-Baptiste Sauvan for fruitful discussions. AD and RF are supported by the German

Federal Ministry for Education and Research (BMBF) under contract no. 05H24WWA. The research of DL has been supported by the Italian Ministry of Universities and Research (MUR) under the FIS grant (CUP: D53C24005480001, FLAME). GP acknowledges support from the EU Horizon Europe research and innovation programme under the Marie-Sklodowska Curie Action “POEBLITA - POLarised Electroweak Bosons at the LHC with Improved Theoretical Accuracy” - grant agreement no. 101149251 (CUP H45E2300129000).

References

- [1] CMS collaboration, *Measurement of vector boson scattering and constraints on anomalous quartic couplings from events with four leptons and two jets in proton–proton collisions at $\sqrt{s} = 13$ TeV*, *Phys. Lett. B* **774** (2017) 682 [[1708.02812](#)].
- [2] CMS collaboration, *Evidence for electroweak production of four charged leptons and two jets in proton–proton collisions at $\sqrt{s} = 13$ TeV*, *Phys. Lett. B* **812** (2021) 135992 [[2008.07013](#)].
- [3] ATLAS collaboration, *Observation of electroweak production of two jets and a Z-boson pair*, *Nature Phys.* **19** (2023) 237 [[2004.10612](#)].
- [4] ATLAS collaboration, *Differential cross-section measurements of the production of four charged leptons in association with two jets using the ATLAS detector*, *JHEP* **01** (2024) 004 [[2308.12324](#)].
- [5] CMS collaboration, *Vector Boson Scattering prospective studies in the ZZ fully leptonic decay channel for the High-Luminosity and High-Energy LHC upgrades*, Tech. Rep. CMS-PAS-FTR-18-014, CERN, Geneva (12, 2018).
- [6] B. Jäger, C. Oleari and D. Zeppenfeld, *Next-to-leading order QCD corrections to Z boson pair production via vector-boson fusion*, *Phys. Rev. D* **73** (2006) 113006 [[hep-ph/0604200](#)].
- [7] F. Campanario, M. Kerner, L.D. Ninh and D. Zeppenfeld, *Next-to-leading order QCD corrections to ZZ production in association with two jets*, *JHEP* **07** (2014) 148 [[1405.3972](#)].
- [8] B. Jäger, A. Karlberg and G. Zanderighi, *Electroweak ZZjj production in the Standard Model and beyond in the POWHEG-BOX V2*, *JHEP* **03** (2014) 141 [[1312.3252](#)].
- [9] C. Li, Y. An, C. Charlot, R. Covarelli, Z. Guan and Q. Li, *Loop-induced ZZ production at the LHC: An improved description by matrix-element matching*, *Phys. Rev. D* **102** (2020) 116003 [[2006.12860](#)].
- [10] A. Denner, R. Franken, M. Pellen and T. Schmidt, *NLO QCD and EW corrections to vector-boson scattering into ZZ at the LHC*, *JHEP* **11** (2020) 110 [[2009.00411](#)].
- [11] A. Denner, R. Franken, M. Pellen and T. Schmidt, *Full NLO predictions for vector-boson scattering into Z bosons and its irreducible background at the LHC*, *JHEP* **10** (2021) 228 [[2107.10688](#)].
- [12] A. Ballestrero, E. Maina and G. Pelliccioli, *Polarized vector boson scattering in the fully leptonic WZ and ZZ channels at the LHC*, *JHEP* **09** (2019) 087 [[1907.04722](#)].
- [13] D. Buarque Franzosi, O. Mattelaer, R. Ruiz and S. Shil, *Automated predictions from polarized matrix elements*, *JHEP* **04** (2020) 082 [[1912.01725](#)].
- [14] M. Hoppe, M. Schönherr and F. Siegert, *Polarised cross sections for vector boson production with Sherpa*, *JHEP* **04** (2024) 001 [[2310.14803](#)].
- [15] A. Denner, S. Dittmaier, M. Roth and D. Wackeroth, *Predictions for all processes $e^+e^- \rightarrow 4$ fermions + γ* , *Nucl. Phys.* **B560** (1999) 33 [[hep-ph/9904472](#)].
- [16] A. Denner, S. Dittmaier, M. Roth and L.H. Wieders, *Electroweak corrections to charged-current $e^+e^- \rightarrow 4$ fermion processes: Technical details and further results*, *Nucl. Phys.* **B724** (2005) 247 [[hep-ph/0505042](#)].
- [17] A. Denner and S. Dittmaier, *The complex-mass scheme for perturbative calculations with unstable particles*, *Nucl. Phys. Proc. Suppl.* **160** (2006) 22 [[hep-ph/0605312](#)].

- [18] A. Denner and S. Dittmaier, *Electroweak Radiative Corrections for Collider Physics*, *Phys. Rept.* **864** (2020) 1 [[1912.06823](#)].
- [19] R.G. Stuart, *Gauge invariance, analyticity and physical observables at the Z^0 resonance*, *Phys. Lett. B* **262** (1991) 113.
- [20] A. Aeppli, G.J. van Oldenborgh and D. Wyler, *Unstable particles in one loop calculations*, *Nucl. Phys.* **B428** (1994) 126 [[hep-ph/9312212](#)].
- [21] A. Denner, S. Dittmaier, M. Roth and D. Wackerroth, *Electroweak radiative corrections to $e^+e^- \rightarrow WW \rightarrow 4$ fermions in double pole approximation: The RACONWW approach*, *Nucl. Phys.* **B587** (2000) 67 [[hep-ph/0006307](#)].
- [22] A. Denner and G. Pelliccioli, *Polarized electroweak bosons in W^+W^- production at the LHC including NLO QCD effects*, *JHEP* **09** (2020) 164 [[2006.14867](#)].
- [23] A. Denner and G. Pelliccioli, *NLO EW and QCD corrections to polarized ZZ production in the four-charged-lepton channel at the LHC*, *JHEP* **10** (2021) 097 [[2107.06579](#)].
- [24] A. Denner, C. Haitz and G. Pelliccioli, *NLO EW and QCD corrections to polarised same-sign WW scattering at the LHC*, *JHEP* **11** (2024) 115 [[2409.03620](#)].
- [25] CMS collaboration, *Measurements of production cross sections of polarized same-sign W boson pairs in association with two jets in proton-proton collisions at $\sqrt{s} = 13$ TeV*, *Phys. Lett. B* **812** (2021) 136018 [[2009.09429](#)].
- [26] ATLAS collaboration, *Evidence for Longitudinally Polarized W Bosons in the Electroweak Production of Same-Sign W Boson Pairs in Association with Two Jets in pp Collisions at $\sqrt{s} = 13$ TeV with the ATLAS Detector*, *Phys. Rev. Lett.* **135** (2025) 111802 [[2503.11317](#)].
- [27] S. Catani and M.H. Seymour, *A general algorithm for calculating jet cross-sections in NLO QCD*, *Nucl. Phys.* **B485** (1997) 291 [[hep-ph/9605323](#)].
- [28] Z. Nagy and Z. Trócsányi, *Next-to-leading order calculation of four-jet observables in electron-positron annihilation*, *Phys. Rev.* **D59** (1999) 014020 [[hep-ph/9806317](#)].
- [29] S. Dittmaier, *A general approach to photon radiation off fermions*, *Nucl. Phys.* **B565** (2000) 69 [[hep-ph/9904440](#)].
- [30] S. Catani, S. Dittmaier, M.H. Seymour and Z. Trócsányi, *The dipole formalism for next-to-leading order QCD calculations with massive partons*, *Nucl. Phys.* **B627** (2002) 189 [[hep-ph/0201036](#)].
- [31] S. Dittmaier, A. Kabelschacht and T. Kasprzik, *Polarized QED splittings of massive fermions and dipole subtraction for non-collinear-safe observables*, *Nucl. Phys.* **B800** (2008) 146 [[0802.1405](#)].
- [32] L. Basso, S. Dittmaier, A. Huss and L. Oggero, *Techniques for the treatment of IR divergences in decay processes at NLO and application to the top-quark decay*, *Eur. Phys. J. C* **76** (2016) 56 [[1507.04676](#)].
- [33] A. Denner, S. Dittmaier, M. Pellen and C. Schwan, *Low-virtuality photon transitions $\gamma^* \rightarrow f\bar{f}$ and the photon-to-jet conversion function*, *Phys. Lett.* **B798** (2019) 134951 [[1907.02366](#)].
- [34] A. Denner, D. Lombardi, S. Lopez Portillo Chavez, M. Pellen and G. Pelliccioli, *MoCaNLO: a Monte Carlo integrator for NLO calculations*, [2602.19842](#).
- [35] A. Denner, R. Franken, C. Haitz, D. Lombardi and G. Pelliccioli, *Electroweak corrections to doubly polarised WZ scattering at the LHC*, *JHEP* **02** (2026) 120 [[2510.26462](#)].
- [36] A. Denner, D. Lombardi, S. Lopez Portillo Chavez, M. Pellen and G. Pelliccioli, *Mocanlo*, Feb., 2026. [10.5281/zenodo.19829093](#).
- [37] S. Actis, A. Denner, L. Hofer, A. Scharf and S. Uccirati, *Recursive generation of one-loop amplitudes in the Standard Model*, *JHEP* **04** (2013) 037 [[1211.6316](#)].

- [38] S. Actis, A. Denner, L. Hofer, J.-N. Lang, A. Scharf and S. Uccirati, *RECOLA: REcursive Computation of One-Loop Amplitudes*, *Comput. Phys. Commun.* **214** (2017) 140 [[1605.01090](#)].
- [39] A. Denner, S. Dittmaier and L. Hofer, *COLLIER: a fortran-based Complex One-Loop Library in Extended Regularizations*, *Comput. Phys. Commun.* **212** (2017) 220 [[1604.06792](#)].
- [40] F.A. Berends, R. Pittau and R. Kleiss, *All electroweak four fermion processes in electron-positron collisions*, *Nucl. Phys.* **B424** (1994) 308 [[hep-ph/9404313](#)].
- [41] S. Dittmaier and M. Roth, *LUSIFER: A LUCid approach to six FERmion production*, *Nucl. Phys.* **B642** (2002) 307 [[hep-ph/0206070](#)].
- [42] PARTICLE DATA GROUP collaboration, *Review of particle physics*, *Phys. Rev. D* **110** (2024) 030001.
- [43] D. Bardin, A. Leike, T. Riemann and M. Sachwitz, *Energy-dependent width effects in e^+e^- -annihilation near the Z-boson pole*, *Physics Letters B* **206** (1988) 539.
- [44] LHC HIGGS CROSS SECTION WORKING GROUP collaboration, *Handbook of LHC Higgs Cross Sections: 4. Deciphering the Nature of the Higgs Sector*, *CERN Yellow Rep. Monogr.* **2** (2017) 1 [[1610.07922](#)].
- [45] S. Dittmaier and M. Krämer, *Electroweak radiative corrections to W-boson production at hadron colliders*, *Phys. Rev.* **D65** (2002) 073007 [[hep-ph/0109062](#)].
- [46] NNPDF collaboration, *Photons in the proton: implications for the LHC*, *Eur. Phys. J. C* **84** (2024) 540 [[2401.08749](#)].
- [47] CMS collaboration, *Measurement of the ZZ production cross section and $Z \rightarrow \ell^+ \ell^- \ell'^+ \ell'^-$ branching fraction in pp collisions at $\sqrt{s} = 13$ TeV*, *Phys. Lett. B* **763** (2016) 280 [[1607.08834](#)].
- [48] Y.L. Dokshitzer, G.D. Leder, S. Moretti and B.R. Webber, *Better jet clustering algorithms*, *JHEP* **08** (1997) 001 [[hep-ph/9707323](#)].
- [49] M. Cacciari, G.P. Salam and G. Soyez, *The anti- k_t jet clustering algorithm*, *JHEP* **04** (2008) 063 [[0802.1189](#)].
- [50] A. Denner and S. Pozzorini, *One-loop leading logarithms in electroweak radiative corrections. 1. Results*, *Eur. Phys. J.* **C18** (2001) 461 [[hep-ph/0010201](#)].
- [51] Z. Bern et al., *Left-handed W bosons at the LHC*, *Phys. Rev.* **D84** (2011) 034008 [[1103.5445](#)].
- [52] W.J. Stirling and E. Vryonidou, *Electroweak gauge boson polarisation at the LHC*, *JHEP* **07** (2012) 124 [[1204.6427](#)].